J Mater Sci: Mater Electron (2017) 28:9245–9251
DOI 10.1007/s10854-017-6659-2

Morphological and local magnetic properties of cobalt clusters electrodeposited onto indium tin oxide substrates

M. Rivera[1] · F. I. Martinez-Vado[1] · L. H. Mendoza-Huizar[2] · O. Amelines-Sarria[3] · I. Betancourt[4]

Received: 16 December 2016 / Accepted: 25 February 2017 / Published online: 18 March 2017

Abstract Magnetic force microscopy was employed in order to investigate the local magnetic distribution of individual cobalt clusters electrodeposited onto indium tin oxide surfaces. In addition, the size and shape of the clusters were analyzed by using scanning electron microscopy and atomic force microscopy at various electrodeposition potential values or growth stages. From these results, the cluster magnetic state at different cluster dimensions was identified and the critical cluster size for the magnetic transition from the single to the multi domain state was obtained. By analyzing the local magnetic states of the aggregates in terms of a theoretical single-domain ferromagnetic model, various magnetic parameters were inferred. Finally, in order to validate the experimental results, a micromagnetic simulation study was employed which correctly confirmed the experimental magnetic transition diagram, and also, provided some insights of other intrinsic magnetic properties of the aggregates.

✉ M. Rivera
mrivera@fisica.unam.mx

[1] Dpto. Materia Condensada, Instituto de Física, Universidad Nacional Autónoma de México, Ciudad Universitaria, Coyoacán, C.P. 04510 Mexico, DF, Mexico

[2] Mineral de la Reforma, Centro de Investigaciones Químicas, Universidad Autónoma del Estado de Hidalgo, C.P. 42181 Pachuca, Hidalgo, Mexico

[3] Facultad de Ingeniería Mecánica, Universidad Pontificia Bolivariana, Autopista Piedecuesta Km 7, Bucaramanga, Colombia

[4] Dpto. Materiales Metálicos y Cerámicos, Instituto de Investigaciones en Materiales, Universidad Nacional Autónoma de México, Ciudad Universitaria, Coyoacán, C.P. 04510 Mexico, DF, Mexico

1 Introduction

Cobalt systems exhibit a wide range of magnetic properties that can be used in modern technological applications such as data storage devices, sensor and actuator technology, recording heads, high-performance permanent magnets, and transformer steel sheets, among others. In recent years, cobalt clusters and thin films have been grown on various substrates, since it is well known that the presence of a substrate determines not only the size and shape of the cluster, but also its intrinsic physical and chemical properties below certain nanometer range [1].

In particular, for practical applications such as magnetic storage media, it is required that grains remain independent in order to maintain low coupling and high anisotropy among them. As the size of the grains increases and their proximity decreases, the exchange coupling plays an important role to determine the aggregate or film magnetic behavior [2]. Therefore, it is crucial to understand the relationship between the size and shape with the magnetic characteristics of individual aggregates.

Nowadays, there are different techniques to grow cobalt clusters onto different substrates [3–6]. Nevertheless, electrochemical methods have become an interesting alternative since through a suitable combination of bath and control parameters, it is possible to regulate their population, dimension and crystalline properties [7, 18]. On the other hand, the electrode substrate also plays a key role in the nucleation and growth mechanisms of these grains. For instance, it has been shown that Co nanoparticles can be electrodeposited onto vitreous carbon [9], SiO2 [10], gold [11], glassy carbon (GCE) [12], highly oriented pyrolitic graphite (HOPG) [13–15], indium tin oxide (ITO) [16], and Nb surfaces [17], among others, with particular crystalline structures and magnetic properties. Unfortunately, one

important aspect that has not been fully investigated is the magnetic evolution of these clusters grown onto solid substrates at different growth stages.

On the other hand, magnetic force microscopy has become an important tool to study magnetic stray field distributions on clusters and thin films with high spatial resolution. In a previous report, it was observed that cobalt electrodeposits from sulfate solutions onto highly oriented pyrolytic graphite electrodes (HOPG) showed a clear relationship between the size and the local magnetic properties of aggregates as a function of the electrodeposition bath composition [8]. In a later work, the local magnetic state of cobalt clusters electrodeposited from sodium sulfate solutions onto HOPG was correlated with the height and diameter of the clusters. Here, the magnetic transition from the mono to the multi domain state was obtained and clearly depended on the high rather than the diameter of the aggregate [18]. In addition, by employing complementary theoretical and micromagnetic modelling studies, intrinsic magnetic parameters of the clusters such as the exchange constant, anisotropy, and crystalline state (fcc) were inferred.

Therefore, in order to further investigate the substrate influence on the nucleation, local magnetic state and magnetic transition of electrodeposited cobalt clusters, a magnetic force microscopy (MFM) study was carried. In this work, indium tin oxide (ITO) was employed as a working electrode substrate since this substrate is one of the most widely used surfaces for technological applications. The experimental results were validated theoretically and by using a micromagnetic simulation program, local intrinsic magnetic parameters of the aggregates were inferred. It is clear, that this information will contribute to the understanding of fundamental aspects of magnetic nanoclusters, and therefore, its potential technological applications.

2 Experimental

The electrochemical experiments were performed in a conventional three electrode cell. Cobalt aggregates were electrodeposited onto indium tin oxide (ITO) electrodes from the sulfate aqueous solution 10^{-2} M of $CoSO_4 + 1$ M Na_2SO_4 at room temperature. It has been observed that this particular bath composition has shown an overall quality of the electrodeposits, since Na + ions do not react electrochemically at the electrode surface, producing larger nanoparticles with better magnetic properties [8]. The solution was prepared by using analytic reagent grade products with ultra pure water (18 MOhms, Simplicity Millipore system). The solution was deoxygenated by bubbling N_2 for 15 min before each experiment. The electrochemical experiments were carried out in a BAS Epsilon potentiostat connected to a personal computer running the EPSILON-EC electrochemical analyzer software. In this work, a graphite bar and a saturated silver electrode (Ag/AgCl) were used as counter and reference electrodes, respectively. Cyclic voltammetry experiments were carried out at 20 mV/s in order to identify the cobalt reduction potential for the system. Finally, the cobalt clusters were obtained by using the potential step technique from +600 mV towards different reduction potential values (−820, −840, −860, −880, −900, and −920 mV) for 32 s. From previous experience with this electrochemical system, it was found that by using these perturbation potential values and formation time, a diffusional 3D growth was obtained [18].

The clusters characterization was performed immediately after formation with a scanning electron microscope (SEM) JEOL JSM5600 LV coupled with a Noran X-ray microanalysis system for the Energy Dispersive Spectroscopy (EDS) analysis. The SEM studies were carried out at 20 keV. Atomic Force Microscopy (AFM) and Magnetic Force Microscopy (MFM) images were obtained simultaneously with a JEOL JSPM 4210 microscope. The magnetic MFM tips were MikroMasch magnetic probes with a Co-Cr magnetic coating. All tips were magnetized along the pyramid axis prior to the scanning process. In MFM images, the bright and dark contrast regions correspond to repulsive and attractive forces, respectively, which in turn represent domains with up or down out-of-plane magnetization. In order to avoid morphological information from contaminating the magnetic measurements, large tip-sample distances (lift heights) were employed. This number was well above 10 nm, which is considered the upper limit where van der Waals forces become significant [19].

3 Theoretical and micromagnetic modeling studies

In order to investigate the relationship between the clusters magnetic states and their dimensions, a theoretical single domain ferromagnetic model was employed. In 1988, Aharoni derived a rigorous theory to describe the magnetic properties of elongated single-domain ferromagnetic particles [20]. Although there are different models to investigate the transition of magnetic nanoclusters, this particular approach employs a geometric analysis in terms of the size and shape of the aggregates. These characteristics can be easily obtained by using microscopy probe techniques, and allowed us to accurately describe the local magnetic properties of each cluster. The main assumption of this model is that single domain states are well characterized for elongated particles by only using a magnetostatic term F_0 given by

$$F_o = \frac{1}{2} N_R M_s^2 \upsilon \quad (1)$$

where υ is the volume, M_s the saturation magnetization and N_R a demagnetizing factor which depends on the aspect ratio m, where $m = a/d$ being a the length of the minor axis and d the length of the major axis of an elongated particle. Therefore, under these conditions, there is a critical dimension (a_o) below which the particles exhibit a single domain magnetic state. The theoretical expression for this parameter is:

$$a_0 = \frac{1.84}{M_S} \left(\frac{A}{N_R} \right)^{\frac{1}{2}} \quad (2)$$

where A is the exchange constant [21].

In addition, in order to obtain a predicted magnetic state of clusters with different dimensions, the finite difference (FD) micromagnetic simulation program OOMMF [22] was employed. In this program, the Landau–Lifshitz-Gilbert equation was numerically solved to calculate the equilibrium out-of-plane magnetic component in order to compare with MFM images.

For the simulations, the saturation magnetization (M_S) of cobalt (M_s=1.42×10^6 A/m) [23] and the magnetocrystalline anisotropy $K_1 = 4.1 \times 10^5$ J/m^3 [24] were employed as independent parameters, whereas the exchange constant (A) was used as a fitting parameter. Finally, the damping constant α was 1.0 in order to improve convergence in a reasonable number of iterations since only the final magnetic state of the cluster was required. The simulations where performed on ellipsoids with base diameters ranging from 50 to 350 nm and heights from 5 to 25 nm. These interval values were determined from individual clusters as seen with atomic force microscopy. The simulations were carried out in the presence of a uniform external magnetic field (380 mT) applied along the z direction, in order to simulate the presence of the magnetic MFM tip [18]. The cluster mesh was 2.0 nm, which was below the calculated exchange length value by using $L_{ex} = \left(2A/\mu_0 M_s^2\right)^{1/2} = 2.7$nm [24], with $A = 1.1 \times 10^{-11}$ J/m [25].

Once the converge torque value reached the stopping criterion of 1e-5 relative to Ms, the magnetic states in the z direction of the clusters were analyzed in order to characterize the local magnetic distribution and plot the magnetic transition diagram.

4 Results and discussion

In Fig. 1, the cyclic voltammetry response of systems ITO/0.01 M CoSO4 + 1.0 M Na_2SO_4 is shown. In this case,

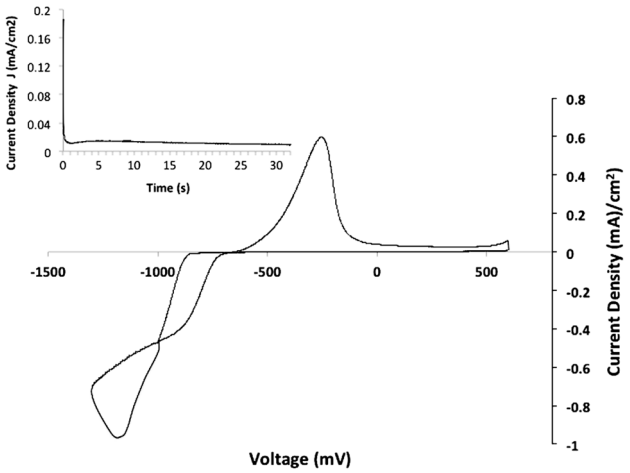

Fig. 1 Cyclic voltammetry plot of the ITO/Co system from a sulfate solution. The *inset* shows the chronoamperometric plot

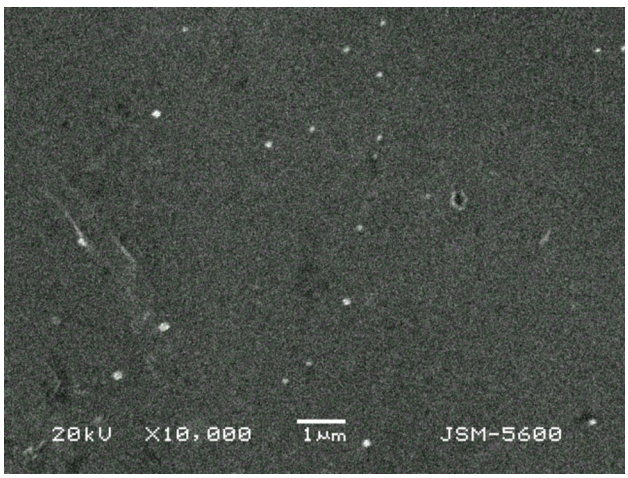

Fig. 2 SEM image of the ITO surface after Co electrodeposition. *Inset* figure contains the elemental analysis

only anodic and cathodic peaks are observed which are related to a cobalt deposition and dissolution.

From this information, the cobalt potential interval for deposition was identified in order to study the cobalt nucleation and growth by using chronoamperometric methods. The transients were obtained by applying a + 0.600 V initial potential at six different reduction potential values in the interval from −820 to −920 mV to investigate the initial stages of cluster formation. The inset in Fig. 1 corresponds to the chronoamperometric plot at −840 mV. In all cases, the chronoamperometric information suggested a bidimensional followed by a tridimensional cobalt growth with an average nucleation speed of 2.062 nuclei cm^{-2} s^{-1}.

In Fig. 2, a SEM image of the electrode after deposition with the −840 mV voltage is shown. Here, a very regular

surface can be seen. From this image, a very homogenous ITO surface with no obvious clusters, defects or large aggregates is observed. The inset in this figure, exhibits an EDS analysis, which shows the typical ITO/glass substrate elements plus cobalt. On the other hand, in Fig. 3 AFM images of the ITO surface are show. For instance, in Fig. 3a an AFM topographic image shows a typical instantaneous nucleation phenomenon, with the presence of individual clusters on the ITO surface with similar diameters and heights. From the statistical measurements of the cluster dimensions, most of the clusters exhibit polyhedral shapes. In the case of irregular forms with elongated-type shapes, the largest in-plane length was selected as the representative dimension (or diameter) of the cluster. The height and diameter intervals of the aggregates were found to be between 2 and 9 and 5–700 nm, respectively. From this image, it is observed that most of the clusters are isolated from each other, but in some case, the coalescence of two or more cluster is easily identified.

Figure 3b shows the magnetic image of the ITO/cobalt surface. The *contrast colors* in this image is evident. The surface shows a homogenous *dark color*, whereas the aggregates show a *clear light contrast* that evidences the presence of a magnetic material. By comparing Fig. 3a, b, it is possible to identify the position of some of the clusters in both images, but the presence of others is only appreciated in the magnetic figure where the shape of the aggregates can be clearly observed, but more important, the *color tone* within the clusters changes depending on the size of the aggregates.

It is worth noticing that the presence of one single color can be more easily appreciated in small aggregates, while two or more color contrast regions can be observed in aggregates of larger size. This results, suggest the presence of single and multi magnetic states, respectively. In Fig. 4, a statistical analysis of the size of the aggregates at different potential formations is shown. Figure 4a corresponds to the diameter while Fig. 4b to the height of the clusters. From these plots, it is clear that the diameter of the cluster increases as the potential increases, this is, the average diameter of most of the clusters for the lowest −820 mV potential formation grow from 140 to 370 nm for the largest potential value at −920 mV. On the other hand, the height decreases as the potential augments as seen in Fig. 4b. The average height for the clusters formed at −820 mV is 8 nm while this number decreases to 3.8 nm for the −920 mV formation value. During absorption, a nucleation is achieved in different substrate

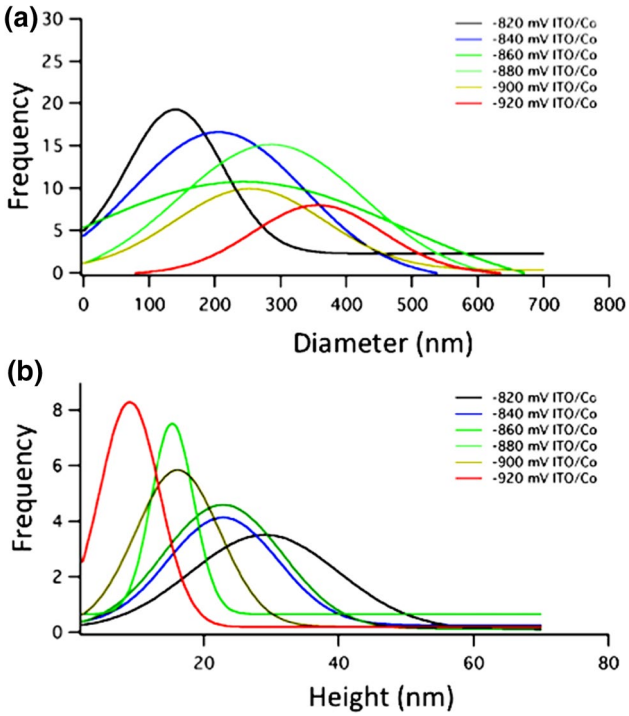

Fig. 4 Frequency histogram of the **a** diameter and **b** height of the clusters at different formation potentials

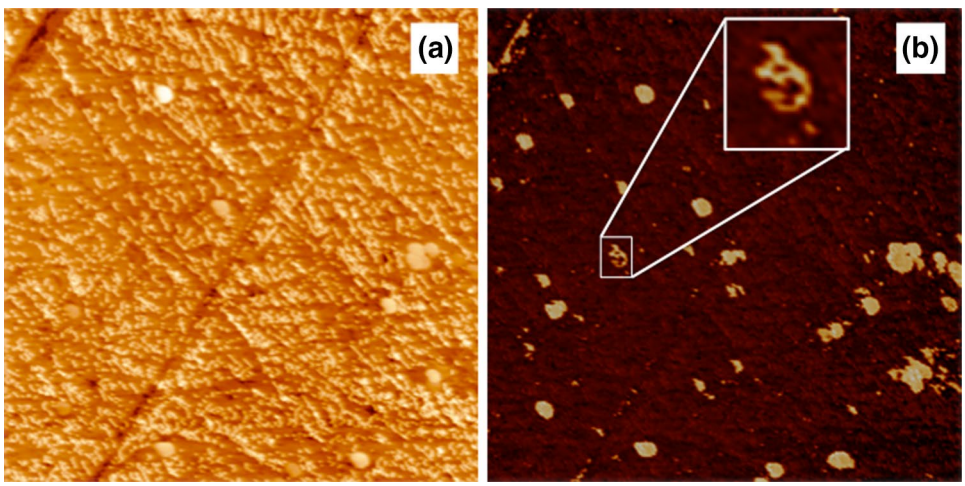

Fig. 3 **a** AFM and **b** MFM images of the ITO surface, where the presence of magnetic material is clearly observed. The magnetic images also shows a cluster with multimagnetic regions. Image sizes are 10 x 10 μm

positions. As the potential increases, the cobalt nuclei absorb preferentially to the ITO surface and then migrate to the already formed clusters increasing their diameter. Since this is an instantaneous nucleation phenomena, the higher the formation potential, the larger the amount of nuclei and size of the clusters. The roughness analysis of the surface in Fig. 5 shows that as the potential formation increases, the number of nuclei or islands increases too, and therefore, the roughness becomes higher. At higher potential values, as more atoms are absorbed on the electrode surface the diameter of the islands augments due to cobalt diffusion in the direction parallel to the electrode surface. In addition, there is an absorption and coalescence of atoms, which form a monolayer, decreasing the apparent height of the clusters, and therefore, the roughness value. For much higher potential values, the next stage would be the growth of new islands on top of the newly formed layer. This growth behavior is typical of an instantaneous nucleation phenomenon.

In Fig. 6, the plot of the diameter versus height for the clusters at −820 mV potential formation is shown. Here, different individual clusters where analyzed in terms of its size and magnetic state as seen from MFM. It is clear that single domain states remain in the lower left side of the graph, while the multi domain states are more randomly distributed above certain height. The same behavior was observed for all other potential values and even the critical height was nearly the same. From the experimental plots, the critical height for the single to multi domain transition was in average 6 nm. It is interesting to notice that this critical height for the single to multi domain transition is lower than the one observed for the same electrodeposition bath but using a different substrate (HOPG) [18]. This suggests that the interaction of the ITO substrate with the cobalt aggregates is slightly weaker in comparison with the graphite surface.

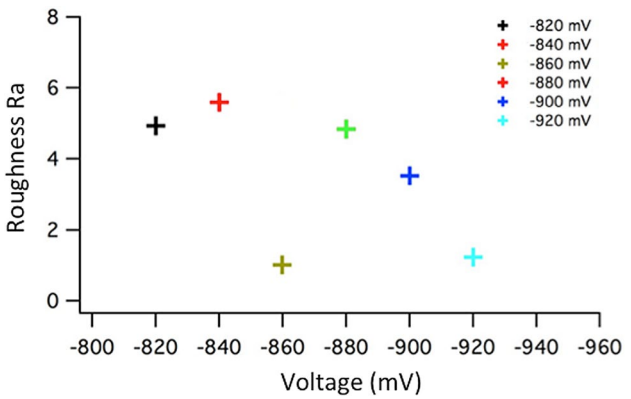

Fig. 5 Roughness analysis of the ITO surface at different formation potentials

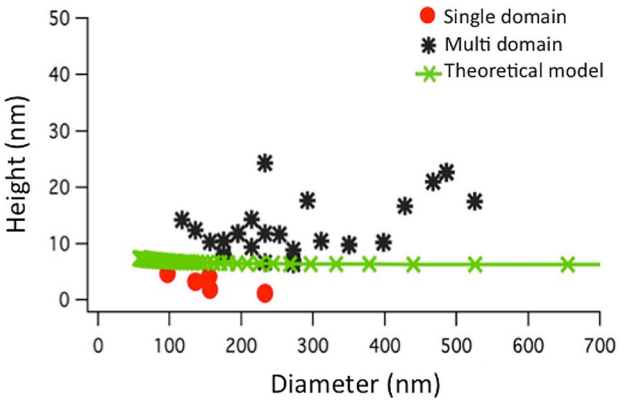

Fig. 6 Experimental magnetic states observed by MFM as a function of the height and the diameter of the clusters. *Dots* represent single domains while *stars* represent multi domains. The *solid line* represents the theoretical lower boundary for the magnetic transition from the theoretical model

In order to find the best fitting plot for each of the formation potential, Eq. 2 was employed by using the exchange constant value as a fitting parameter. In Table 1, the fitted exchange constant value for each potential is shown.

The exchange constant value of bulk cobalt is 1.0×10^{-11} J/m [24]. As we can see from Table 1, the largest exchange constant is nearly 3 times smaller than the cobalt bulk value. By looking at the general trend of the exchange constant as a function of the potential formation, it is clear that A decreases as the diameter of the cluster increases. In a previous work by Dumas et al., they found that cobalt clusters assembled as thin films on Si(100) substrates, exhibited a similar exchange constant value, $A=2.3\times10^{-12}$ J/m [25], for cobalt cluster diameters of 9.3 nm. They suggest that this reduction may be attributed to the reduce density of the cluster film or changes in the exchange energy due to alterations of the structural properties at boundaries between clusters [23]. An additional aspect derived from the variation of A is the diminishing of the Curie temperature T_c for decreasing A, since $T_c \propto A$ within the frame of mean field

Table 1 Electrodeposition potential voltage with the corresponding exchange constant A fitted value from Eq. (2)

Potential formation value (mV)	Exchange constant A [J/m] × 10^{-12}
−820	2.87
−840	2.41
−860	2.59
−880	2.38
−900	2.16

approximation [25]. In other words, as the Co clusters become smaller, their Curie temperature enhances over their bulk counterpart reference value.

By using the cobalt saturation magnetization $M_s=1.42\times10^6$ A/m^3 and m = a/d with a the height and d the diameter of the cluster, the theoretical lower bound was obtained and plotted as a solid line in Fig. 6. This plot clearly agrees with the critical height for the transition and predicted $a_o=6$ nm in agreement with the experimental results. Consistent results were obtained for all the electrodeposition voltages. The exchange constant values theoretically obtained for each potential were employed for the simulations. From these plots, we can clearly observed that the single domain magnetic clusters remained always below the theoretical critical size, while the multi magnetic domain aggregates were always above this value as seen in Fig. 6. A similar behavior was observed on cobalt nanoclusters electrodeposited onto monocrystalline silicon [23].

In Fig. 7, the transition diagram for the single to the multi domain magnetic transition calculated with the micromagnetic program is shown. In order to construct this diagram, only the out-of-plane magnetization was analyzed to compare with MFM results. The single domain showed a uniform color while the multi domain state exhibited various contrast regions, as indicated also in Fig. 7 by two examples of simulated clusters above and below the critical height for single domain formation. The simulations

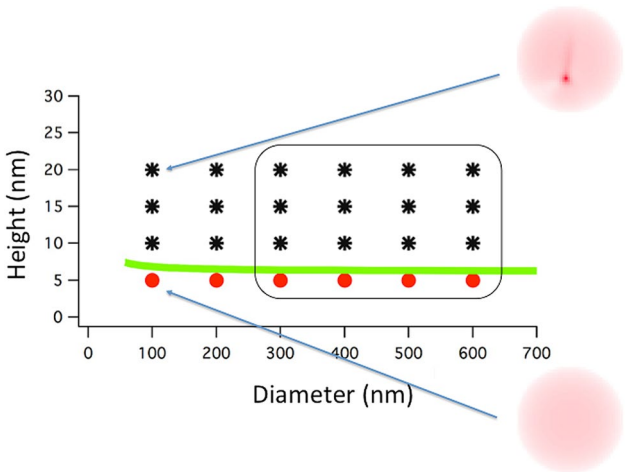

Fig. 7 Calculated magnetic diagram of the out-of-plane magnetic component obtained with OOMMF. *Dots* represent single domain states while *stars* represent multi domain states for different diameters and heights. The theoretical curve was included for comparison with Fig. 6. In addition, the *rectangle* represents the clusters calculated with elongated shapes in contrast with circular forms. Two examples of simulated clusters are included, showing on one hand, a single domain state (without contrast) for a cluster with 100 nm diameter and 5 nm height, and, on the other hand, a cluster with 100 nm diameter and 20 nm height showing inner contrast, which represent a multidomain configuration

were initially performed on spheroids with base diameters ranging from 50 to 600 nm and heights from 5 to 20 nm in order to simulate the experimental shapes at lower formation potentials. Unfortunately, after a cluster diameter of 300 nm, it was very difficult to reproduce the experimental transition diagram, so it was decided to modify the shape of the aggregates. So, for clusters with diameters higher than 300 nm, elongate spheroids with a 2:1 ratio were employed. After this modification, the experimental transition diagram was fully reproduced. This result is consistent with the experimental shapes found in the morphological analysis, where small aggregates showed semicircular shapes, while large aggregates exhibited elongates figures.

For the micromagnetic calculations, it is worth to mention that we used homogeneous (in-plane) and random initial magnetic states as starting configurations and the results were the same regardless of the initial state. On the other hand, we used the exchange constant values (A) obtained from the theoretical model as well as different crystalline structures in order to fit our experimental results. From our analysis, we found that the crystalline structure that fitted our experimental values corresponded to a faced-centered cubic (fcc) phase with a magnetic anisotropy value of 2.17×10^5 J/m^3. It is interesting to notice that the best fitted-magnetic anisotropy was closer to the bulk fcc Co rather than the most common bulk hcp Co value [26]. Other groups have observed that cobalt electrodeposited onto different substrates from sulfate solutions exhibit both hexagonal close-packed (hcp) and faced-centered cubic (fcc) structures [27, 28]. The preferential crystalline orientation of the electrodeposited Co nanostructures seems to be related to the bath composition, electrodeposit parameters, temperature and type of substrate, among others.

5 Conclusions

Isolated cobalt aggregates were obtained onto ITO surfaces by using cronoamperometric methods from sulfate solutions at different formation potential values. The cobalt nucleation was instantaneous and the clusters exhibited different magnetic states depending on the cluster size. MFM results agree with theoretical predictions where the presence of a critical high determines the transition between single to multi magnetic domain aggregates. By analyzing the clusters magnetic configuration with a theoretical model in terms of their size, the magnetic exchange constant value was obtained. Although this value was lower that the bulk exchange constant, as the size of the clusters increased, the exchange constant decreased probably due to structural properties or defects within the clusters. By using micromagnetic simulations, it was possible to reproduce

the experimental transition from single to multi domain aggregates, to infer the fcc crystal structure of the clusters, and to reproduce the shape of the aggregate at different potential values. Finally, by analyzing the local stray field of individual cobalt clusters, it was possible to infer intrinsic magnetic local properties of cobalt aggregates at various growth stages onto ITO surfaces.

Acknowledgements MRH acknowledges Dr. Carlos R. Magaña and M. en C. Jaqueline Cañetas for SEM technical support, Ing. Diego Quiterio for sample preparation assistance, and LCM-IFUNAM for microscopy facilities.

Compliance with Ethical Standards

Conflict of interest The authors declare that they have no conflict of interest.

References

1. C.S.S.R. Kumar (ed), (*Magnetic Nanomaterials*. (Wiley, Weinheim, 2009)
2. E. Miyashita, R. Taguchi, N. Funabashi, T. Tamaki, H. Okuda, IEEE Trans Magn. **38**, 2075 (2002)
3. J.S. Pan, R.S. Liu, Z. Zhang, S.W. Poon, W.J. Ong, S.E. Tok, Surf. Sci. **600**, 1308 (2006)
4. S.A. Koch, R.H. te Velde, G. Palasantzas, J.T. de Hosson, Appl. Phys. Lett. **84**, 556 (2004)
5. C.H. Rios-Reyes, L.H. Mendoza-Huizar, M. Rivera, J. Solid State Electrochem. **14**, 659 (2010)
6. S.W. Poon, J.S. Pan, E.S. Tok, Phys. Chem. Chem. Phys. **8**, 3326 (2006)
7. D. Grujic, B. Pesic, Electrochim. Acta **49**, 4719 (2004)
8. M. Rivera, C.H. Rios-Reyes, L.H. Mendoza-Huizar, Appl. Surf. Sci. **255**, 1754 (2008)
9. E. Gomez, E. Valles, J. Appl. Electrochem **32**, 693 (2002)
10. A.G. Munoz, G. Staikov, Electrochem. Acta, **51**, 2836, (2006)
11. L.H. Mendoza-Huizar, J. Robles, M. Palomar-Pardave, J. Electrochem. Soc. **152**, C265 (2005)
12. L.H. Mendoza-Huizar, C.H. Rios-Reyes, M. Rivera, C.A. Galan-Vidal, Adv. Technol. Mater. Mater. Proc. J. **8**, 152, (2006)
13. C.H. Rios-Reyes, M. Rivera, L.H. Mendoza-Huizar, in *Theoretical and Experimental Advances in Electrodeposition*, ed. by L.H. Mendoza-Huizar (Research SignPost Publishers, 2008), p. 1
14. C.H. Rios-Reyes, L.H. Mendoza-Huizar, M. Rivera, J. Electrochem. Soc. **14**, 659 (2010)
15. L.H. Mendoza-Huizar, C.H. Rios-Reyes, M. Rivera, Quim. Nova **33**, 1109 (2010)
16. H.-Y. Ho, W.-B. Chen, T.-Y. Fu, S.-J. Chen. IEEE Trans. Mag **50**, 2277758 (2014)
17. H.-Y. Ho, S.-J. Chen, W.-Y. Lin, Y. Liou, H.-W. Cheng, IEEE Trans. Magn. **48**, 6332737 (2012)
18. M. Rivera, C.H. Rios-Reyes, L.H. Mendoza-Huizar, J. Magn. Magn. Mater. **323**, 997 (2011)
19. S. Porthun, L. Abelman, C. Lodder, J. Magn. Magn. Mater. **182**, 238, (1998)
20. A. Aharoni, J. Appl. Phys **63**, 5879 (1988)
21. A. Moina, L. Oliveira-Versic de, M. Vazdar, Mater. Let. **58**, 3518–3522, (2004)
22. M.J. Donahue, D.G. Porter, *Interagency Report NISTIR 6376*. (National Institute of Standards and Technology, Gaithersburg, MD, 1999)
23. F. Dumas-Bouchiat, H.S. Nagaraja, F. Rossignol, C. Champeaux, G. Trolliard, A. Catherinot, D.J. Givord, Appl. Phys **100**, 064304 (2006)
24. E. du Trémolet de Lacheisserie, D. Gignoux, M. Schlenker (eds.), *Magnetism: Materials and Applications* (Springer, New York, 2005)
25. D. Jiles (ed.), *Introduction to Magnetism and Magnetic Materials* (CRC Press, Boca Raton, 1998)
26. S. Blundell, *Magnetism in condensed Matter* (Oxford University Press, Oxford, 2001)
27. T.M. Manhaboso, I.L. Muller, J. Mat. Sci. **44**, 2931 (2009)
28. M.R. Khelladi, L. Mentar, A. Azizi, F. Kadirgan, G. Schmerber, A. Dinia, Appl. Sci. **258**, 3907 (2012)